Scientific
Research
Publishing

Computer Simulation/Practical Models for Human Thyroid Thermographic Imaging

James Rizkalla[1], William Tilbury[1], Ahdy Helmy[2], Vinay Kumar Suryadevara[3], Maher Rizkalla[3], Michael M. Holdmann[3]

[1]Indiana University School of Medicine, Indianapolis, IN, USA
[2]Indiana University School of Medicine/VA Hospital, Indianapolis, IN, USA
[3]Department of Electrical and Computer Engineering, Purdue School of Engineering and Technology, Indianapolis, IN, USA
Email: mrizkall@iupui.edu

Abstract

We have demonstrated a successful computer model utilizing ANSIS software that is verified with a practical model using Infrared (IR) sensors. The simulation model incorporates the three heat transfer coefficients: conduction, convection, and radiation. While the conduction component was a major contributor to the simulation model, the other two coefficients have added to the accuracy and precision of the model. Convection heat allows for the influence of blood flow within the study, while the radiation aspect, sensed through IR sensors, links the practical model of the study. This study also compares simulation data with the applied model generated from IR probe sensors. These sensors formed an IR scanner that moved via servo mechanical system, tracking the temperature distribution within and around the thyroid gland. These data were analyzed and processed to produce a thermal image of the thyroid gland. The acquired data were then compared with an Iodine uptake scan for the same patients.

Keywords

1. Introduction

Medical imaging analysis is being applied to biological techniques with high capability and decreasing costs. Advanced computers and data acquisition systems enhance the processing speed and data accuracy, leading to better imaging. In addition, advances in microelectronics and System on Chip (SOC) have made sensors with

phenomenal sensitivities within advanced equipment [1]. High-tech solid-state device sensors are allowing accurate non-invasive diagnosis in many medical imaging systems. Non-invasive methods of diagnosis are allowing more patients to be screened for a variety of disease conditions. The information gathered from various techniques may serve to rule out or confirm a diagnosis.

This work also emphasizes the different image modalities for thyroid gland screening. Thyroid disorders are the second most common in endocrine pathology. Nearly 8% - 20% of the adult population worldwide experience thyroid-related diseases, of which, fewer than 5% are diagnosed with cancer. Graves' disease is a common cause of hyperthyroidism that affects a great deal of individuals. Proper diagnosis may impact the efficiency and cost of treatment [2].

The clinical symptoms of thyroid disease may include hyperthyroidism with certain differential diagnosis including thyroiditis and iodine deficiency, in addition to Graves' disease and toxic nodules. The normal thyroid looks homogeneous with uniform distribution and no apparent hyper cellularity or enlargement. While Iodine^{123} uptake has some advantages with regard to the imaging of the thyroid, such as better electron capture and gamma energy (159 Kev), there are still issues with high radiation precursors, short half-lives, and high cost. Thyroid nodules may be categorized as cold nodules (nonfunctioning), hot nodules (functioning), or indeterminate. Cold nodules indicate a decreased uptake by a solitary nodule, often warranting a biopsy for further investigation. Fine needle aspiration (FNA) is the method of choice for biopsy intending to identify potential adenomas or carcinomas. Furthermore, acute thyroiditis may be designated from cold nodule for the focal abscess. Hot nodules may produce a great deal of hormone leading to hyper-functioning, resulting in hyperthyroidism (Graves' disease), nodular goiter, or even thyrotoxicosis. The thyroid is a highly vascular organ supplied by arteries such as the superior thyroid artery, branching off the external carotid, and the inferior thyroid artery from the thyrocervical trunk of the subclavian artery. Additionally, the thyroid's venous system is comprised of the superior, middle, and inferior thyroid veins. All of these vessels result in the thyroid's extremely vascular network. These vessels may marginally contribute in transmitting thermal energy that may impact the thermography of the thyroid diagnosis. The following radionuclides in **Table 1** [3] are used in imaging with varying properties that are useful for various diagnosis.

Universally, there are several methods of medical diagnostic imaging in use. These include X-rays, ultrasonography, computed tomography (CT), positron emission tomography (PET), magnetic resonance imaging (MRI), nuclear medicine, and thermography. Generally speaking, X-ray diagnostic method is mostly used to produce images of bones structures, although with low power or intensity it is sometimes used to diagnose soft tissue disorder. X-rays are high-energy photons that can pass through materials (impeded based on energy levels) and can cause severe damage to living tissue. Therefore, human exposure to X-rays must be carefully monitored and limited. A second imaging technique uses ultrasonography, which is based on the propagation characteristics of acoustic waves in the body rather than electromagnetic waves. This modality is usually faster and less expensive, and no ionizing radiation is involved. It drives energy at the upper limit of the human hearing. By transmitting short pulses of ultrasound into the body and detecting the echoes from tissue interfaces, an image of internal structures can be produced. There are a number of scanning modes, including amplitude scan, time motion scan, brightness scan, real time scan, Doppler measurement, duplex scan, and supplementary scanning for 3-D image production. Various image processing software are useful in enhancing ultrasound images. A third imaging method is by computed tomography (CT), commonly known as "CAT scan", involves acquiring many X-ray images from different angles that may be processed to reconstruct a 3-D view for the area of interest. The fourth imaging technique is the Positron emission tomography (PET), which combines the use of a radio labeled substance and computed tomography with a gamma camera. This facilitates the measurement of an organ's function, rather than its size or shape. It uses small amount of radioactive material as compared to X-ray, which makes preferable to physicians. The PET process includes production of positron emitting isotope in a cyclotron, labeling

Table 1. Radionuclides used in imaging.

Type	Means	Dose	Half-Life	Energy
99m Tc	IV	2 - 10 mCi	6.0 Hrs	140 KeV
I^{123}	Oral	200 - 400 µCi	13.6 Hrs	159 KeV
I^{131}	Oral	30 - 100 µCi	8.05 days	364 keV

and preparing compound in a form suitable for administration in humans, transport of the labeled compound from chemistry group to camera group, injection of tracer compound and data acquisition with PET camera, processing the data from the PERT to extract information related to tracer's kinetics in the body, and finally, interpreting the results. A fifth method of imaging is the Magnetic Resonance Imaging (MRI), a technique that uses very strong magnetic field (typically 3 Tesla) and radio waves to take multiple cross-sectional images of the body, which then assembled into a three-dimensional image by a computer. MRI is one of the best tests available for obtaining detailed look at some of the organs in the body. It is particularly useful in imaging the brain, spine, and joints. A unique advantage of MRI is the ability to image in different planes, leading to 3D coordinate system. It provides high soft tissue contrast, and use of non-ionizing radiation, permitting normal subjects to be scanned. MRI imaging however, have high costs and poor image artifacts from respiratory and cardiac motion. A sixth method for imaging is the thermography. This type deals with the detection, recording, and display of natural heat emission, a widely used technique in industry. As it applies to the medical field, it is the measurement and display of temperature distribution of the body surface. There are two different types of thermography used in medicine: contact and non-contact. The contact method usually employs flexible sheets of liquid crystals. These crystals change color within narrow temperature ranges. When the material is placed in direct contact with the surface of the skin, the change in crystal color provides a thermal map of the skin. This technique suffers from the effective heat sinking properties of the sheets, however. Therefore, it is generally used for qualitative thermography. The non-contact method is a non-invasive technique that measures heat radiating in the infrared region of the spectrum. Infrared cameras operate by focusing this energy on one or more crystal. When these materials absorb heat energy, a change in their resistance may be detected.

2. Comparison between Imaging Modalities

When comparing imaging modalities, many various factors contribute to which modality will be utilized. The reliability and accuracy comes first in considering what modality will be utilized. **Table 2** below gives summary of the comparison between the 6 imaging modalities mentioned above with respect to their primary use, features, limitations, and cost [3].

3. Thermography Applications in Medicine

Thermal imaging has been applied to many fields, including peripheral vascular pathologies and cancer diagnosis [4] [5], and breast pathologies [6] [7]. It is also widely used in the chiropractic field. It has also been used to detect problems associated with gynecology [8], dermatology [9], heart, and brain. Recent efforts have emphasized temperature distribution of regions of interest and for detection of abnormalities. Thermal images of the

Table 2. Comparison of imaging modalities.

Imaging method	Application	Features	Limitations	Cost
X-Ray	Bone structures (soft tissues at low intensity	Widely available	Radiation exposure	$300
Ultrasound	Soft tissue	Widely available Accessible, noninvasive, quick, highly sensitive	Echo problems, quality, interpretation of images, inferior to cross-sectional imaging in identifying lymphadenopathy extension thyroid disease	$100
CT	Brain disorders	3-D view	Contrast agent injection required for thyroid imaging and 4 - 6 weeks wait after Iodine scan. Radiation exposure is also an issue	$800
PET	Brain Disorders	Functional view of process		$2000
MRI	Nodules as small as 4 mm detected, normal thyroid homogeneous signal intensity slightly greater than neck musculature brain and joints	Well defined view contrast agent	Injection is required for thyroid imaging	$1000
Nuclear medicine	Organ and glandular diagnosis	Functional view of process	Injection is required for thyroid imaging and cant use on pregnant women	$800
Thermography	Vascular diseases	Non-invasive	Small penetration	$100

human skin contain a tremendous amount of clinical information, and unlike many other imaging modalities, thermography is a harmless and non-invasive technique that quantitatively measures spatial and temporal abnormalities in blood perfusion of the skin. Because the hyperactive nodule is a center of increased blood flow and increased hormones production, it should be also a center of heat production, which is detectible by thermal sensing.

Thermal diagnosis of thyroid is based on the study of the temperature distribution of the hot nodule. Several thyroid disorders are possible in humans. The patient may be suffering from a toxic nodule, multiple nodule toxic goiters, or diffuse hyperactivity of the thyroid gland. In order to distinguish between these possibilities, the physician would normally request a radiolabeled iodine scan. Hyperthyroidism during pregnancy presents special concerns for pregnant women because the excess hormone crosses the placenta and adversely affects the fetus. Also the radiolabelled Iodine can destroy the fetus thyroid. A safer diagnostic method might supply useful supplementary information. Recent development in thermal imaging may utilize the readily available components and subsystems for a non-invasive, safe, and cost effective proto-type.

4. Thermography Devices

In order to map the temperature distribution on the skin of the neck, several types of temperature transducers may be employed. This may include contact thermocouples, non-contact infrared thermocouples, RTDs, thermistors, and liquid crystal sensors. The advantages and disadvantages of each type of transducers are presented in **Table 3** below along with the measuring parameters for each device.

Some of the issues that must be considered when selecting the thermal sensors include degree of thermal contact, the temperature of neighboring objects, the dissipated heat by the sensor elements, and the mass of the sensor. Most of these issues may be addressed by the self powered infrared (IR) thermocouples. Similar to the visible light, IR radiation obeys the basic laws of refraction, reflection, diffraction, and polarization that apply to other types of electromagnetic radiation such as UV, X-ray, sound, and radio waves. As it can be seen that the practical limits for temperature measurement via IR is generally accepted as range of 0.75 to 30 microns. The temperature range and plank's law of Radiant energy are given in **Table 4** and **Figure 1**. The data presented here assisted with the selection of the IR devices that would be appropriate for the research. The table discusses about the dependence of the wavelength lambda in microns with respect to temperature ranging from room temperature to 5000°C is presented.

5. Simulation Models for Thermography

In order to design a system that is capable of detecting and mapping temperature distribution of the surface of the skin, the limits of the detector resolution must be determined. This will set the limits on both the type of sensor and the data acquisition system chosen. FEA (finite element analysis) method is a common engineering tool used to solve partial differential equations it is the heat equation in this case. This should determine how much temperature deviation there is likely to be. This will actually set the criteria of what sensor resolution is required and allow for proper choice of a sensor to meet the testing specifications. The approach starts by determining the amount of heat that a normal thyroid gland would generate, then the excess energy generated by the hyperactive thyroid of a nodule. This should give the incremental change in temperature distribution surrounding the tissue underneath the skin in order for the difference to be detectable at the skin's surface. Not counting

Table 3. Comparison of various transducers/sensor types.

Device	Measure parameter	Advantages	Disadvantages
Thermocouple	Voltage resistance	Simplicity, durability, low cost	Low voltage signal required reference, less sensitive, and least stable
RTD	Resistance	Accurate, stable, linear	Self heating, Low output signal, fragile, low absolute, resistance, required current source
Thermistor	Resistance	Fast response High O/P, 20 wire ohms than thermocouple	Non linear Limited temperature range
Liquid crystal sensor	Color change	Durable, Resistance sensitive	Limited temperature range

Table 4. Wien's displacement law for a range of temperature values.

°C	°K	Lambda
27	300	9.6
29	302	9.6
31	304	9.5
33	306	9.4
35	308	9.4
37	310	9.3
40	313	9.2
100	373	7.8
500	773	3.7
1000	1273	2.3
2000	2273	1.3
2727	3000	1.0
5000	5273	0.6
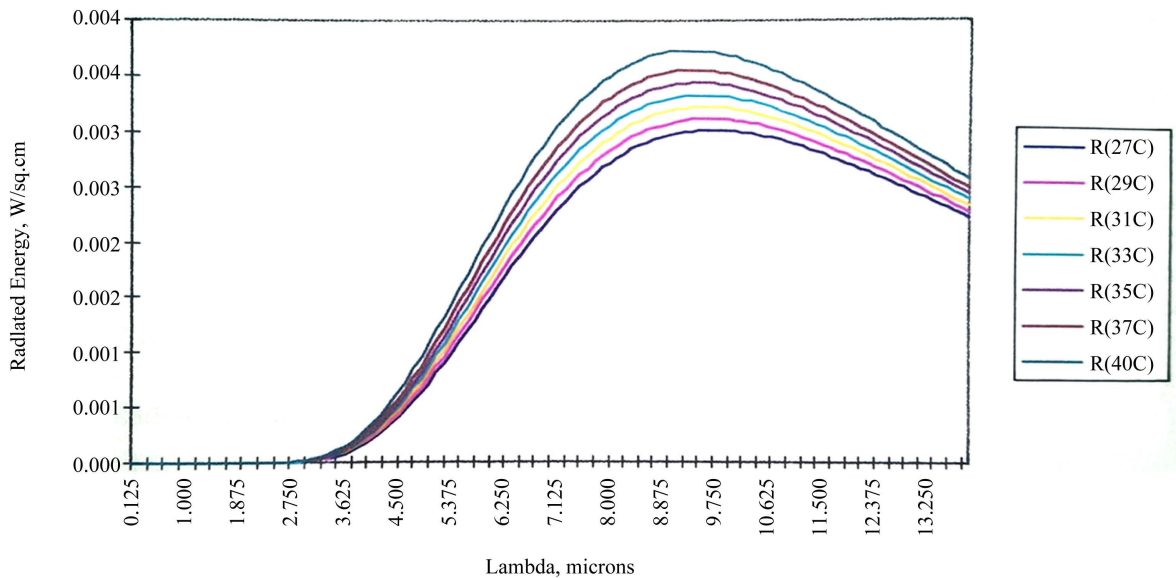
Figure 1. Planks radiation law plot near human body temperatures.

the impact of the blood flow, the model will be simple but limited in accuracy. That model considers only the conduction component of the heat transfer. The heating and cooling effects of blood flow in the capillaries of the skin were not considered. Helmy *et al.* [10] have simulated a simple model of 25 mm thickness of skin with an embedded 10 mm diameter hot nodule. This work is extended to include both the convection and radiation effects of the hot spot. The convection component is developed from the blood vessels, while the radiation is attributed to the IR sensor probe that is distant from the human skin surface. For our research we have designed a model with a 25 mm thick piece of skin and 30 mm × 30 mm square with an embedded 10 mm diameter hot module in ANSYS workbench. The properties for the skin are given to the cuboidal structure and the properties for the thyroid are given to the embedded sphere. The model is finally meshed for simulation with 19,767 nodes and 11,248 triangular surface meshes. **Figure 2** depicts the cuboidal structure and the embedded circular gland.

At steady state, the heat lost to the external environment must balance the heat produced by the human body. The heat loss occurs by several heat transfer modes: radiation, evaporation, convection, and conduction. The environmental situations and metabolic conductions may govern the extent to which each node dominates. The human body must lose the excess heat it produces or a fever condition would result. An estimate of the temperature rise, which would occur in the body if no heat, is dissipated, and can be derived from the definition of the specific heat. The heat flux [11], *q* is described by

$$q = mc_p \Delta t ,$$

where *m* is the mass, Δt is the temperature difference, and c_p is the specific heat. We have considered varied specific heats for skin muscle and the thyroid gland. Results of computer simulation from finite elements are given in **Figure 3**. In this simulation the ambient surface temperature is assumed to be 25˚C and the model is simulated for both heat transfer and the heat flux by changing the temperatures of the embedded nodule. As determined from reference [3] the embedded energy within the nodule may present up to 3˚C temperature change, while keeping the normal temperature the surface of the body. Cooling off the neck in order to suppress the thermal noise may alter the starting temperature at the hot spot where the nodule is. **Figures 3-5** give three different sets of temperature distribution, representing 34˚C, 37˚C, and 40˚C. **Figure 3** gives a set of temperatures given at different times (separated by Δt).
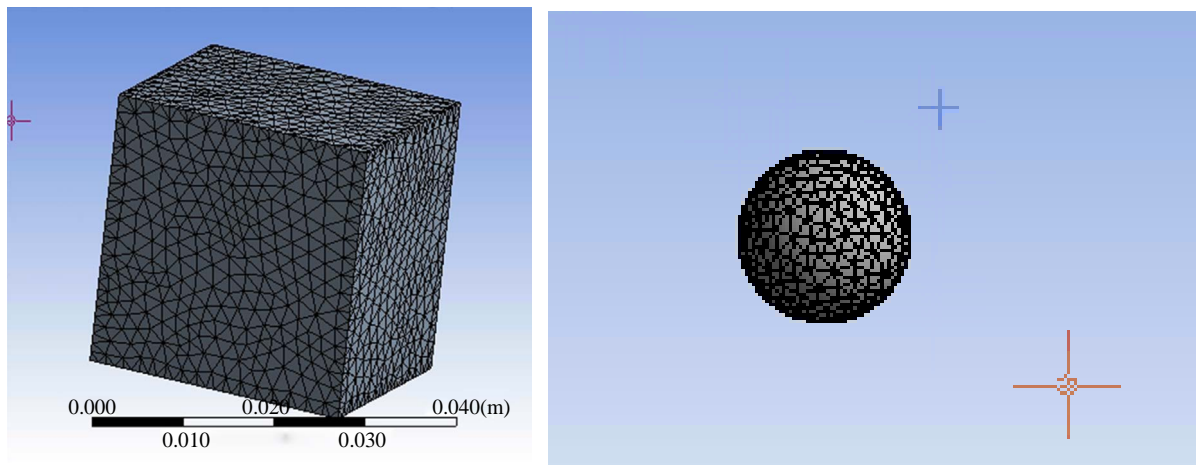

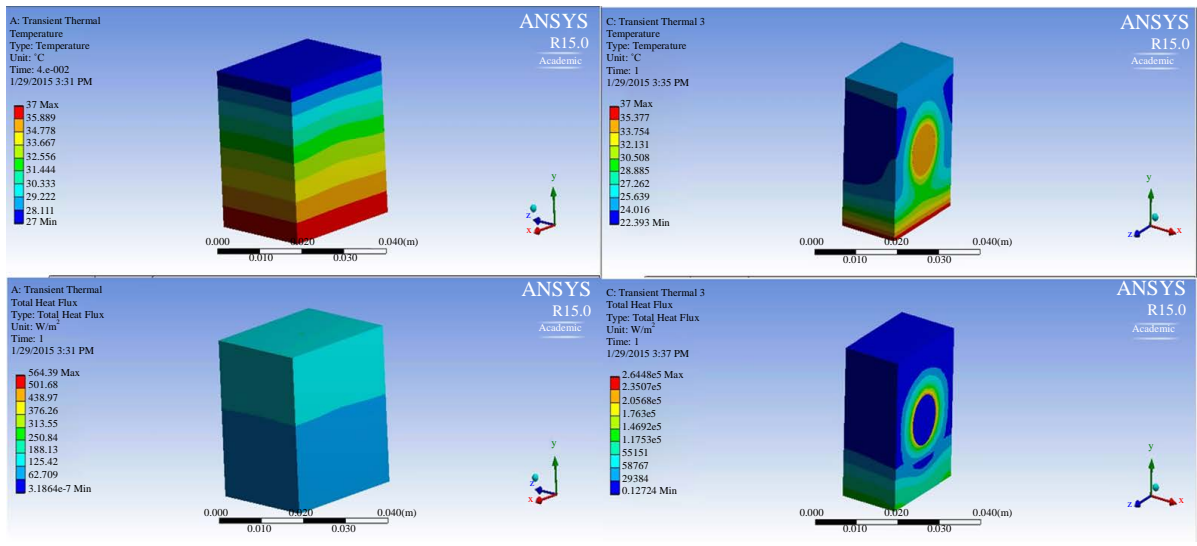**Figure 2.** (a) Structure of the cube; (b) Embedded thyroid gland.

Figure 3. Temperature plot at (a) 34˚C; (b) Sliced view at 34˚C; Heat flux plot at (c) 34˚C; (d) Sliced view 34˚C.
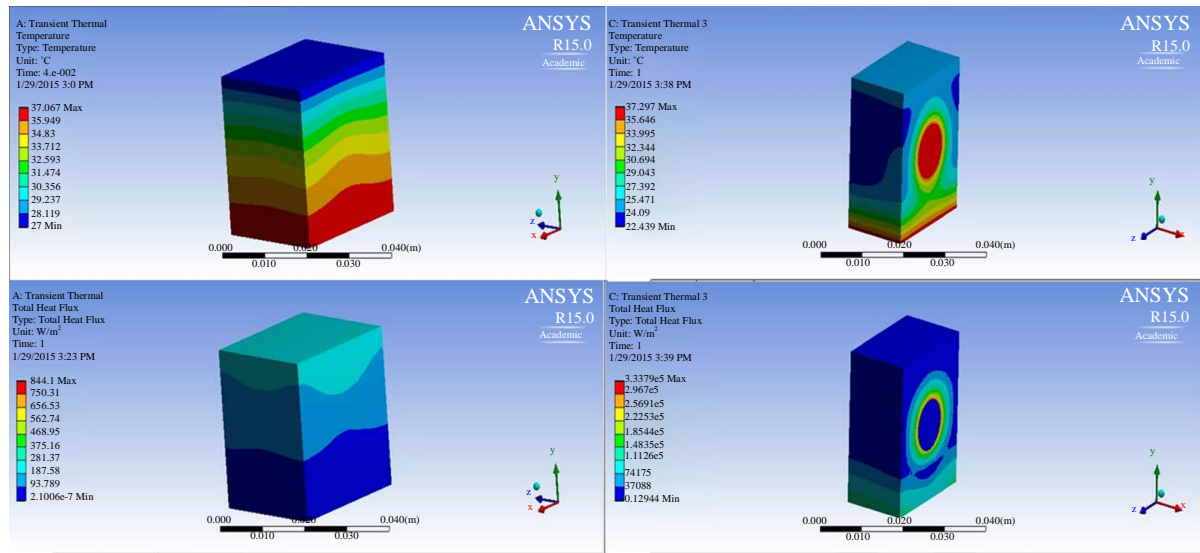
Figure 4. Temperature plot at (a) 37˚C; (b) Sliced view at 37˚C; Heat flux plot at (c) 37˚C; (d) Sliced view 37˚C.
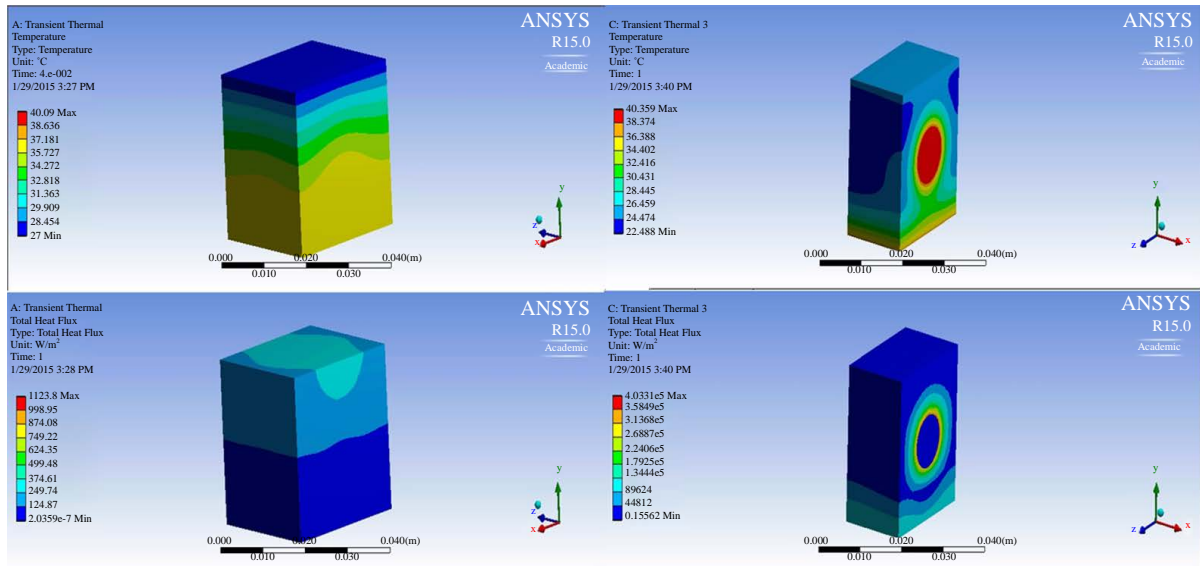

Figure 5. Temperature plot at (a) 40˚C; (b) Sliced view at 40˚C; Heat flux plot at (c) 40˚C; (d) Sliced view 40˚C.

As preliminary estimate of the practicality of thermal sensing the thyroid gland through the skin of the neck, a rough test was devised and implemented. This involved testing the skin temperature on the neck over the thyroid gland of five subjects who had no known thyroid problems (control subjects). **Figure 3** gives a typical set of temperature responses at 11 different positions on the neck surface. The five series give data at different times starting at $t = 0$, where the neck was cold down, for five sets of data separated by few minutes each. As it can be seen from the data, each subject's thyroid lobes can be detected by a rise of temperature at the lobes, with lowered temperature detected in the center of the neck area, that correspond to the isthmus between the two thyroid lobes. This data verifies the localized temperature gradient on the neck. The data also shows that a temperature span of 1.5 - 2 degrees is evident on the skin surface in the area of the thyroid.

6. The Practical Model

The practical system made of eight IR probe connected with servomechanism that is controlled by a stepper motor was used for the data comparison. **Figure 6** shows the practical model.
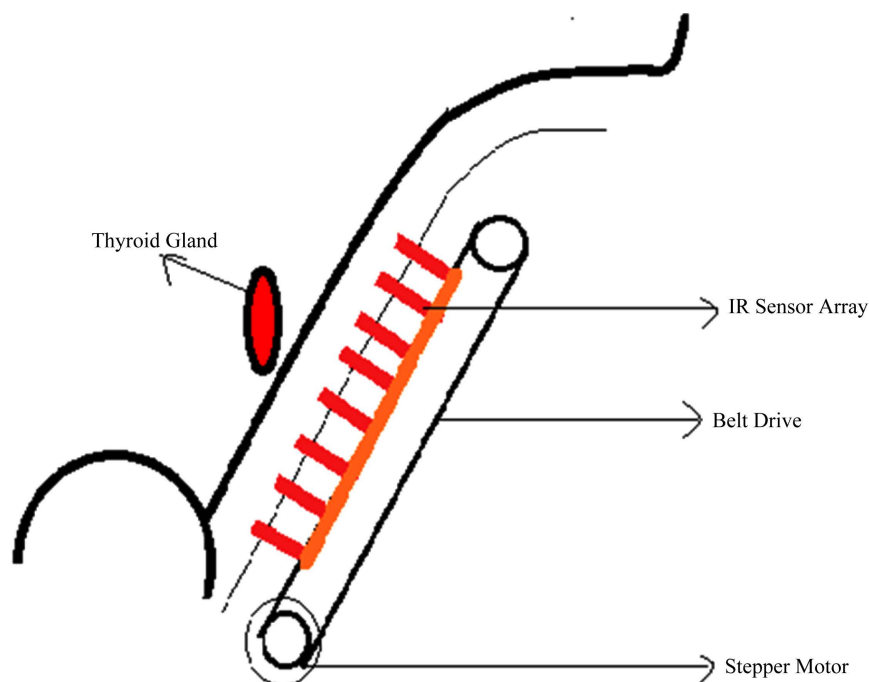
Figure 6. IR probe used for the practical model.

7. Results and Discussions

Figure 7 and **Figure 8** show the gland nodule at different temperatures between 31˚C and 34˚C, and 34˚C to 38˚C. IR sensors have detected nodules with temperature distribution that overlap with the thyroid. **Figure 7**, **Figure 9** shows the thyroid gland with a start of a nodule from the right side of the lobe. **Figure 8** and **Figure 10** shows for multiple cases with multiple nodule case for the same patients. However the thermography device system is a passive system, the institution has gone through the legal process to provide these data. IUPUI informed consent form for the Thyrothermography was taken, covering costs of participating, confidentiality, people to contact, and subject consent. An interdepartmental communication was also taken with IRB. These were the endocrinologist patients with case familiarity.

Practical Model Results

The patient's carotid artery is detected by sensor S1, and two thyroid lobes are detected by sensors S3, S5 and S6. This results in apparent separation distance of approximately 4.5 - 5 cm on center. The temperature distribution within the lobes suggests a core heat source for each lobe, with no nodules.

The simulation results that were obtained by assuming a high temperature gland and its heat conduction and radiation parameters were in accordance with the practical results.

8. Conclusion and Future Work

The approaches followed here may be applied to various medical issues such as kidney stones, and nodular related cancers elsewhere. The computer simulation has shown the changes in temperature within the gland directed towards the skin's surface. Heat transfer coefficients including conduction, convection, and radiation have added to the accuracy of the simulation, and assisted in the selection of the IR sensor that would be appropriate for the practical system. In some practical measurements, overlapping in temperature distribution from multiple nodules was clear, and this was attributed to the interference of each IR sensor on other sensors. In some cases, the nodule may be missed from the IR sensor data if the size of the nodule is comparable with the distance between the sensors. Future work should include a software process that guarantees scanning the regions around the gland. This process can be improved via a smart processing algorithm that processes data obtained from the scanned organ and analyzes the cancer tumors at various parts of the body. In the next phase, we
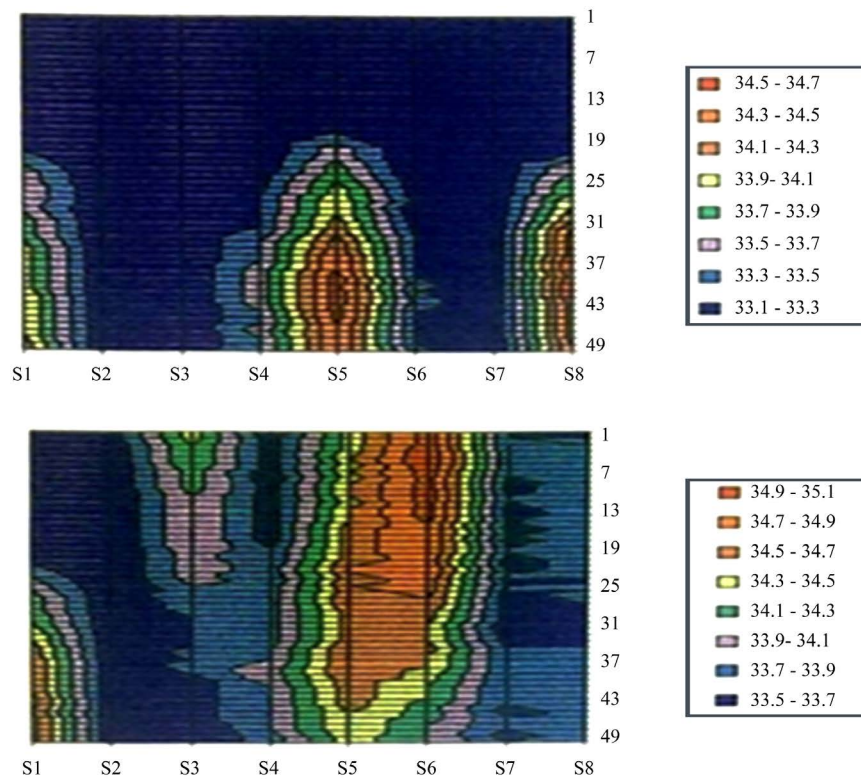
Figure 7. IR thermogram sequence of a patient. Hot spot shows up to 34.5 degrees after cooling off the neck.
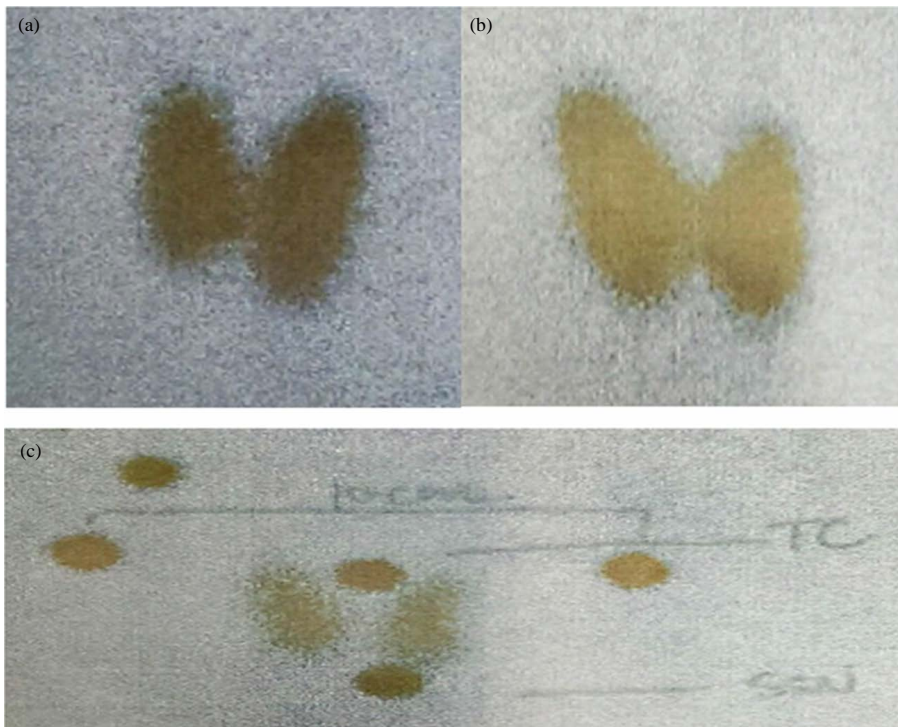
Figure 8. ^{123}I scan-toxic multinodular images. (a) LAO view; (b) RAO view; (c) ANT view at the left side, shows parts of the two gland lobes with 5 nodules around them, corresponding t thermal activities in contrast to relatively lower thermal corresponding.
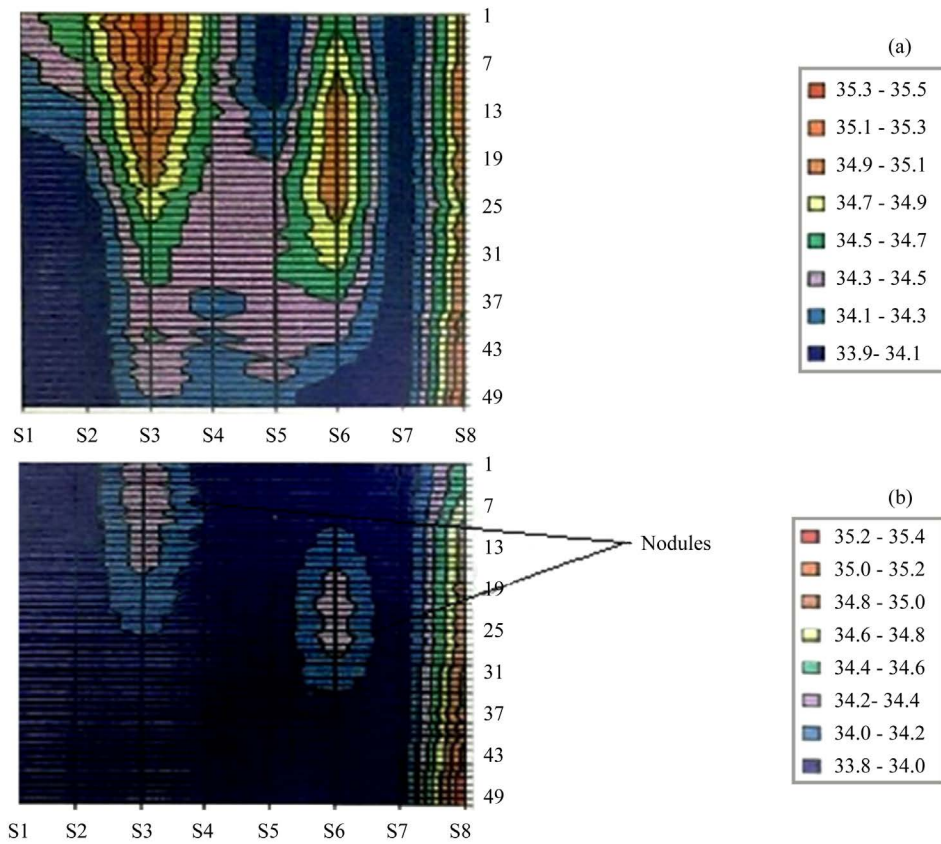
Figure 9. IR thermo gram sequence of a patient. Hot spot shows up to 34.5 degrees after cooling off the neck.
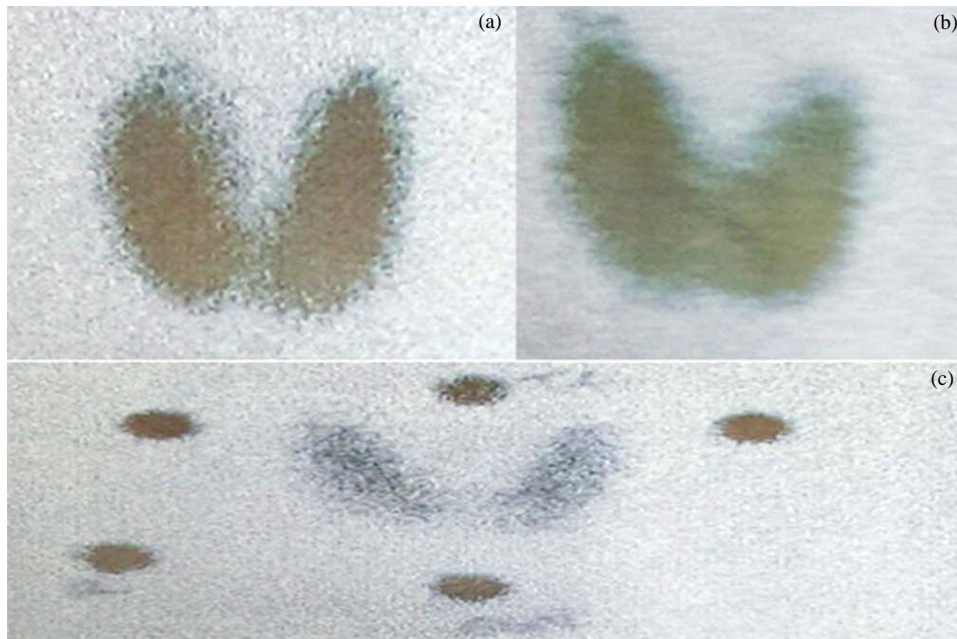
Figure 10. [123]I scan-toxic multinodular images. (a) LAO view; (b) RAO view; (c) ANT view at the left side (**Figure 10(c)**), shows parts of the two gland lobes with 5 nodules around them, corresponding to nodule thermal activity in contrast to relatively lower thermal surroundings.

are planning to develop an efficient IR sensing array of nano-sensors to acquire high-resolution scanning data. The parameters that effect the nano-sensing, such as noise due to ambient parameters, are reduced by placing the sensor array in a vacuum chamber along with liquid nitrogen coolant for maintaining a low-temperature sensor. The sensing apparatus will consist of a sensing array connected to a dedicated processor for initial processing of the data. The data will then be transmitted via WIFI to the host computer. In the future, we are planning to build a smart and integrated remote monitoring system to collect the data from the sensor system. Furthermore, this will be sent to a designated super computer electronically for additional analysis using complex algorithms and GPUs. These initiatives are reserved for future considerations. This will also be a new advancement in the wireless health field, thereby encouraging remote health monitoring systems.

References

[1] Al Khatib, I., Poletti, F., Bertozzi, D., Benini, L., Bechara, M., Khalifeh, H., Jantsch, A. and Nabiev, R. (2006) A Multiprocessor System-on-Chip for Real-Time Biomedical Monitoring and Analysis: Architectural Design Space Exploration. *Design Automation Conference*, 125-130.

[2] Imntyernational Atomic Energy Agency (IAEA) (2009) Nuclear Medicine in Thyroid Cancer Management: A Practical Approach.

[3] Hopkins, C.R. and Reading, C.C. (1995) Thyroid and Parathyroid Imaging. S*eminars in Ultrasound*, *CT and MRI*, **16**, 279-295. http://dx.doi.org/10.1016/0887-2171(95)90033-0

[4] Bagavathiappan, S., Saravanan, T., Philip, J., Jayakumar, T., Raj, B., Karunanithi, R., Panicker, T.M.R., Korath, M.P. and Jagadeesan, K. (2009) Infrared Thermal Imaging for Detection of Peripheral Vascular Disorders. *Journal of Medical Physics*, **34**, 43-47. http://dx.doi.org/10.4103/0971-6203.48720

[5] Bagavathiappan, S., Saravanan, T., Philip, J., Jayakumar, T., Raj, B., Karunanithi, R., Korath, P. and Jagadeesan, K. (2008) Investigation of Peripheral Vascular Disorders Using Thermal Imaging. *The British Journal of Diabetes & Vascular Disease*, **8**, 102-104. http://dx.doi.org/10.1177/1474651408080020901

[6] Schaefer, G., Zavisek, M. and Nakashima, T. (2009) Thermography Based Breast Cancer Analysis Using Statistical Features and Fuzzy Classification. *Pattern Recognition*, **42**, 1133-1137.

[7] Dai, H., Omer, A.M. and Jiang, G. (2008) The Attempt of Breast Thermography Processing Applying with ITE. *IEEE EMBS International Conference on Information Technology Applications in Biomedicine*, Shenzhen, 30-31 May 2008, 160-163. http://dx.doi.org/10.1016/j.patcog.2008.08.007

[8] Dodde, R., Shih, A. and Advincula, A.P. (2009) A Novel Technique for Demonstrating the Real-Time Subsurface Tissue Thermal Profile of Two Energized Surgical Instruments. *Journal of Minimally Invasive Gynecology*, **16**, 599-603. http://dx.doi.org/10.1016/j.jmig.2009.05.018

[9] Kateb, B., Yamamoto, V., Yu, C., Grundfest, W. and Gruen, J.P. (2009) Infrared Thermal Imaging: A Review of the Literature and Case Report. *Journal of Neuroimage*, **47**, T154-T162. http://dx.doi.org/10.1016/j.neuroimage.2009.03.043

[10] Helmy, A., Holdmann, M. and Rizkalla, M. (2008) Application of Thermography for Non-Invasive Diagnosis of Thyroid Gland Disease. *IEEE Transactions on Biomedical Engineering*, **55**, 1168-1175. http://dx.doi.org/10.1109/TBME.2008.915731

[11] Kreith, F. (1973) Principles of Heat Transfer. 3rd Edition, Intext, New York, 607-608.